Phase Structures and Electromechanical Properties of Differently Oriented Epitaxial $K_{0.5}Na_{0.5}NbO_3$ Thin Films

Q. Li*, L. Liu, Y. Ye, J.B. Lv, H.F. Cao and X.X. Sheng

School of Biomedical Engineering, Xinjiang Second Medical College, Karamay 834000, China

Received: 20.10.2023 & Accepted: 11.01.2024

Doi: 10.12693/APhysPolA.145.175 *e-mail: liqiang8529@163.com

An evolved nonlinear thermodynamic theory is used to investigate the phase structures and electromechanical properties of differently oriented $K_{0.5}Na_{0.5}NbO_3$ thin films. It is revealed that notable distinctions in the phase structure of $K_{0.5}Na_{0.5}NbO_3$ thin films, with decreasing symmetry observed in the order of (111), (001), and (110) orientations, and these microphase structural variances translate into distinct electromechanical properties. Moreover, it is observed that the oriented $K_{0.5}Na_{0.5}NbO_3$ thin films exhibit commendable out-of-plane dielectric and piezoelectric properties around the specific phase boundaries, such as M_{aac}–O_{aa} and Te_c–PE phase boundaries for (001) oriented films, M_{aac}–O_{aa} and Te_c–PE phase boundaries for (110) oriented films, R_{aaa}–PE phase boundary for (111) oriented films. Specifically, near room temperature, the (001) and (110) oriented $K_{0.5}Na_{0.5}NbO_3$ thin films outperform (111) oriented $K_{0.5}Na_{0.5}NbO_3$ thin films in terms of dielectric properties, featuring a dielectric constant exceeding 2500. Furthermore, (001) oriented $K_{0.5}Na_{0.5}NbO_3$ thin films exhibit superior out-of-plane piezoelectric properties compared to other orientations, with a remarkable piezoelectric coefficient d_{33} exceeding 1000 pm/V. These results underscore the significant impact of strain and temperature regulation on electromechanical properties. Meanwhile, by strategically adjusting these parameters, it becomes feasible to fabricate high-properties piezoelectric devices.

topics: termodynamic theory, different orientations, phase structures, electromechanical properties

1. Introduction

Ferroelectric materials are expected to become candidates for the new generation of memory, sensors, infrared detectors, and refrigerators due to their excellent ferroelectric, piezoelectric, pyroelectric, and electrothermal properties. Among many ferroelectric materials, the lead-free material potassium sodium niobate ($K_{(1-x)}Na_xNbO_3$) has attracted more attention [1]. With high piezoelectric coefficients, dielectric constant, and Curie temperature, the lead-free $K_{(1-x)}Na_xNbO_3$ materials are expected to substitute mainstream ferroelectric materials, such as lead zirconium titanate ($PbZr_xTi_{1-x}O_3$) [2]. In the process of producing devices characterized by high efficiency, environmental protection, lightweight, and miniaturization, ferroelectric thin films have been widely used in microelectromechanical systems (MEMS), which mainly rely on their excellent electromechanical properties. The effective methods to improve the electromechanical properties of the film mainly focused on strain engineering, domain engineering, phase transition engineering, and doping [3]. During the growth process of thin films, the internal grains grow along certain specific orientations. This type of growth is called preferred orientation growth, and commonly preferred orientations are (001), (110), and (111). In thin films with different preferred orientations, the misfit strain between the substrate and the film is also different, leading to the discrepancy in electromechanical properties. Therefore, regulating the growth orientation of thin films can change their electromechanical properties, and it belongs to the category of strain engineering.

The research on $K_{(1-x)}Na_xNbO_3$ thin films with different preferred orientations mainly relies on experimental methods. Therefore, Kang et al. [4] have fabricated $K_{0.5}Na_{0.5}NabO_3$ films with a thickness of 320 nm on Pt (111)/SiO_2/Si(100) substrates by sol–gel method, and the crystal evolution of thin films was studied by two different annealing methods. The results showed that the film prepared by K-excess precursor solutions exhibits better ferroelectric properties than the Na-excess solutions. Also, the $K_{(1-x)}Na_xNbO_3$ films have been deposited by pulsed laser deposition (PLD), and the electrical, dielectric, and ferroelectric properties of $K_{(1-x)}Na_xNbO_3$ thin films were investigated. The measured dielectric constant ($\sim$ 531) of $K_{(1-x)}Na_xNbO_3$ thin film was found to be in agreement with the value reported in the literature [5]. Pradhan et al. [6] have investigated

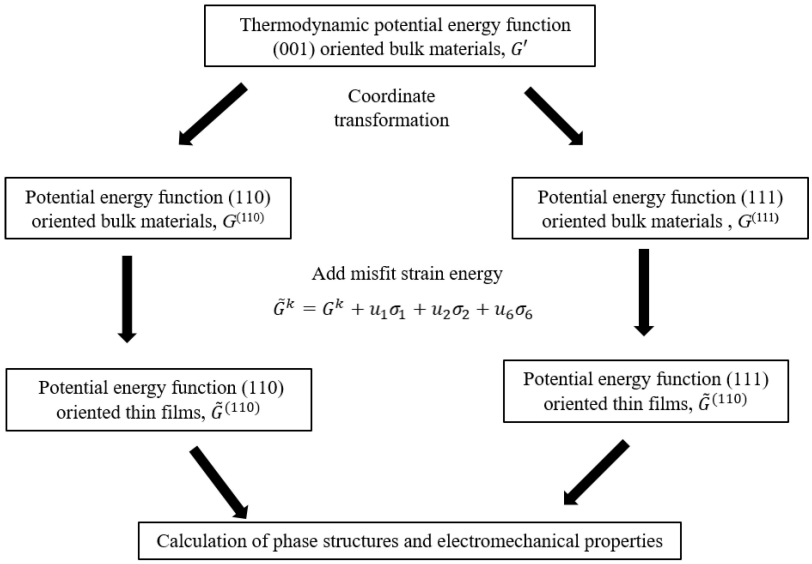

Fig. 1. The diagram of the thermodynamic theoretical framework for this research.

the time dependence of the domain relaxation mechanism in $K_{0.5}Na_{0.5}NbO_3$ thin films grown on $La_{0.67}Sr_{0.33}MnO_3/SrTiO_3$ (001) substrates by a scanning probe microscopy and observed that the $K_{0.5}Na_{0.5}NbO_3$ thin films exhibit excellent charge and domain retention.

In terms of theoretical research, the thermodynamic theory has been widely used in simulating properties of ferroelectric thin films with preferred orientation. For example, Liu et al. [7] have used the machine learning method to predict and classify the temperature–misfit strain phase diagram of (001) oriented $K_{1-x}Na_xNbO_3$ ($0 \leq x \leq 0.5$) thin films, in which the prediction accuracy has reached approximately 99%. Meanwhile, Bai et al. [8] have investigated the electrocaloric effects of (111) oriented $K_{0.5}Na_{0.5}NbO_3$ thin films and found that the maximum electrocaloric $\Delta T \sim 18$ K appears near the phase boundary of ferroelectric–paraelectric phase. Among the above research, it is not difficult to find that there are few researchers using thermodynamic theory to study the electromechanical properties of $K_{(1-x)}Na_xNbO_3$ thin films, because the current research mainly focuses on several materials, such as $(1-x)Pb(Mg_{1/3}Nb_{2/3})O_3 - xPbTiO_3$, $PbZr_xTi_{1-x}O_3$, and $BaTiO_3$ [9–12], however, its thermodynamic potential is limited to sixth-order polynomials and not suitable for materials with eighth-order thermodynamic coefficients, such as $BaZr_xTi_{1-x}O_3$, $Ba_{1-x}Sr_xTiO_3$, and $K_{(1-x)}Na_xNbO_3$, which greatly hinders the prediction of the properties of $K_{(1-x)}Na_xNbO_3$ thin films.

In this article, the eighth-order thermodynamic potential energy functions and the calculation method for electromechanical properties of differently oriented ferroelectric thin films will be derived by transforming order parameters, such as stress, polarization, and electric field. Then, the phase structures and electromechanical properties of differently oriented $K_{0.5}Na_{0.5}NbO_3$ thin films will be studied. The results may provide a basis for the experimental preparation of high-performance capacitors and sensors.

2. Thermodynamic theory

The thermodynamic potential energy and methods for the analysis of electromechanical properties of (001) oriented ferroelectric thin films have been established and well applied. So, in this study, the phase structures and electromechanical properties of (001) oriented $K_{0.5}Na_{0.5}NbO_3$ thin films are explored using the methods described in [7]. Thus, we only need to establish the thermodynamic potential energy and method for calculating electromechanical properties of (110) and (111) oriented ferroelectric thin films. To achieve this purpose, we first establish the global coordinate system $X(x_1, x_2, x_3)$; the x_1, x_2, and x_3 in (110) oriented thin films are along [001], $[1\bar{1}0]$, and [110] direction, while the x_1, x_2, and x_3 in (111) oriented thin films are along $[1\bar{1}0]$, $[11\bar{2}]$, and [111] direction, respectively. Note that x_1 and x_2 are parallel to the film surface, and x_3 is perpendicular to the film surface.

2.1. Thermodynamic potential energies of (110) and (111) oriented thin films

In this part, the potential energy of the (110) and (111) oriented thin films will be deduced by transforming the order parameters of the potential energy of (001) oriented bulk materials and then adding the misfit strain energy. To better explain the subsequent derivation process, we have drawn

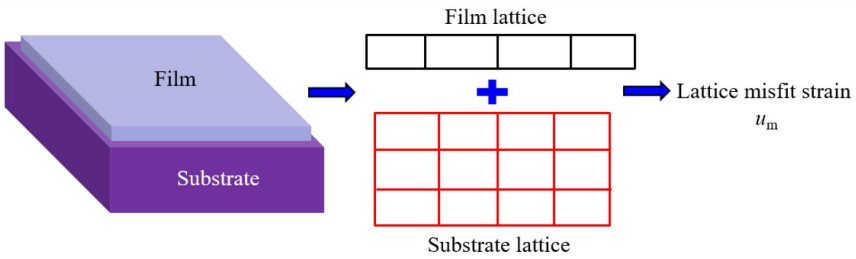

Fig. 2. The schematic diagram of lattice mismatch for the film and substrate.

a diagram of the thermodynamic theoretical framework for this research, as shown in Fig. 1. The specific description of the variables from Fig. 1 will appear in the following text.

Based on Landau–Devonshire theory, considering bulk ferroelectric material under isothermal condition, taking the polarization $P_i^{'}$ $(i = 1, 2, 3)$, stress $\sigma_n^{'}$ $(n = 1, 2, \ldots, 6)$, and electric field $E_i^{'}$ $(i = 1, 2, 3)$ as the order parameters, and using the crystal coordinate system $X'(x_1^{'}x_2^{'}x_3^{'})$ as the reference frame (where $x_1^{'}$ is along [100], $x_2^{'}$ is along [010], and $x_3^{'}$ is along [001], respectively), the thermodynamic potential energy of (001) oriented ferroelectric bulk materials can be expressed as [13, 14]

$$\begin{aligned}
G' = {} & \alpha_1\left(P_1^{'2}+P_2^{'2}+P_3^{'2}\right)+\alpha_{11}\left(P_1^{'4}+P_2^{'4}+P_3^{'4}\right)+\alpha_{12}\left(P_1^{'2}P_2^{'2}+P_2^{'2}P_3^{'2}+P_1^{'2}P_3^{'2}\right) \\
& +\alpha_{111}\left(P_1^{'6}+P_2^{'6}+P_3^{'6}\right)+\alpha_{112}\left[P_1^{'2}\left(P_2^{'4}+P_3^{'4}\right)+P_2^{'2}\left(P_1^{'4}+P_3^{'4}\right)+P_3^{'2}\left(P_1^{'4}+P_2^{'4}\right)\right]+\alpha_{123}P_1^{'2}P_2^{'2}P_3^{'2} \\
& +\alpha_{1111}\left(P_1^{'8}+P_2^{'8}+P_3^{'8}\right)+\alpha_{1112}\left[P_1^{'6}\left(P_2^{'2}+P_3^{'2}\right)+P_2^{'6}\left(P_1^{'2}+P_3^{'2}\right)+P_3^{'6}\left(P_1^{'2}+P_2^{'2}\right)\right] \\
& +\alpha_{1122}\left(P_1^{'4}P_2^{'4}+P_1^{'4}P_3^{'4}+P_2^{'4}P_3^{'4}\right)+\alpha_{1123}\left(P_1^{'4}P_2^{'2}P_3^{'2}+P_2^{'4}P_1^{'2}P_3^{'2}+P_3^{'4}P_1^{'2}P_2^{'2}\right)-\frac{S_{11}}{2}\left(\sigma_1^{'2}+\sigma_2^{'2}+\sigma_3^{'2}\right) \\
& -S_{12}\left(\sigma_1^{'}\sigma_2^{'}+\sigma_2^{'}\sigma_3^{'}+\sigma_1^{'}\sigma_3^{'}\right)-\frac{S_{44}}{2}\left(\sigma_4^{'2}+\sigma_5^{'2}+\sigma_6^{'2}\right)-Q_{11}\left(\sigma_1^{'}P_1^{'2}+\sigma_2^{'}P_2^{'2}+\sigma_3^{'}P_3^{'2}\right) \\
& -Q_{12}\left[\sigma_3^{'}\left(P_1^{'2}+P_2^{'2}\right)+\sigma_2^{'}\left(P_1^{'2}+P_3^{'2}\right)+\sigma_1^{'}\left(P_2^{'2}+P_3^{'2}\right)\right]-Q_{44}\left(P_1^{'}P_2^{'}\sigma_6^{'}+P_2^{'}P_3^{'}\sigma_4^{'}+P_1^{'}P_3^{'}\sigma_5^{'}\right) \\
& -P_1^{'}E_1^{'}-P_2^{'}E_2^{'}-P_3^{'}E_3^{'}, \qquad (1)
\end{aligned}$$

where Q_{IJ} are the electrostrictive coefficients, S_{IJ} are the elastic coefficients, α_1, α_{ij}, α_{ijk}, and α_{ijkl} are dielectric stiffnesses. Note that the temperature-dependent coefficient α_1 can be written as $\alpha_1 = (T - T_0)/(2\varepsilon_0 C)$, in which T_0 is the Curie temperature, C is the Curie constant, and ε_0 is the permittivity of free space. The corresponding thermodynamic coefficients we used, such as α_1, α_{ij}, α_{ijk} and α_{ijkl}, Q_{IJ}, and S_{IJ}, are shown in [15] and [16].

In order to calculate the thermodynamic potential of (110) and (111) oriented bulk materials, it is necessary to transform the stress $\sigma_n^{'}$, polarization $P_i^{'}$, and electric field $E_i^{'}$ under the crystal coordinate system X' in (1) to the corresponding global coordinate system X. The conversion relationship can be expressed as [9, 17]

$$\begin{aligned}
P_i^{'} &= (T^k)^{-1}P_iE_i^{'} = (T^k)^{-1}E_i, \\
\sigma_n^{'} &= (T^k)^{-1}\sigma_n T^k, \qquad (2)
\end{aligned}$$

where the polarization P_i $(i = 1, 2, 3)$, stress σ_n $(n = 1, 2, \ldots, 6)$, and electric field E_i $(i = 1, 2, 3)$ are in global coordinate system X, the superscript "-1" represents the matrix inverse. The matrices T^k are as follows

$$T^{(110)} = \begin{bmatrix} 0 & 0 & 1 \\ \frac{1}{\sqrt{2}} & -\frac{1}{\sqrt{2}} & 0 \\ \frac{1}{\sqrt{2}} & \frac{1}{\sqrt{2}} & 0 \end{bmatrix}, \qquad (3)$$

$$T^{(111)} = \begin{bmatrix} \frac{1}{\sqrt{2}} & -\frac{1}{\sqrt{2}} & 0 \\ \frac{1}{\sqrt{6}} & \frac{1}{\sqrt{6}} & -\frac{2}{\sqrt{6}} \\ \frac{1}{\sqrt{3}} & \frac{1}{\sqrt{3}} & \frac{1}{\sqrt{3}} \end{bmatrix}, \qquad (4)$$

where $T^{(110)}$ and $T^{(111)}$ represent the conversion matrices of (110) and (111) orientation, respectively. Then, substituting the converted polarization $P_i^{'}$, stress $\sigma_n^{'}$, and electric field $E_i^{'}$ into (1), the thermodynamic potential energy functions of (110)

and (111) oriented bulk materials dependent on P_i, σ_n, and E_i can be obtained, denoted as $G^{(110)}$ and $G^{(111)}$, respectively.

For epitaxial thin films, the potential function is also influenced by the misfit strain, resulting from the lattice mismatch between the film and the substrate, as illustrated in Fig. 2. Considering that the thin film grows on a dissimilar cubic substrate and the film surface is free, thus, the misfit strain is an in-plane biaxial misfit strain, and the mechanical boundary obeys the relationship: $u_1 = u_2 = u_m$, $u_6 = 0$, and $\sigma_3 = \sigma_4 = \sigma_5 = 0$, in which $u_m = (b - a_0)/b$, where a_0 and b are the lattice constants of the thin films and substrate, respectively [18]. Thus, introducing the energy caused by the misfit strain, the thermodynamic potential energy of oriented epitaxial thin films can be evolved by the Legendre transformation [18–20]

$$\tilde{G}^k = G^k + u_1\sigma_1 + u_2\sigma_2 + u_6\sigma_6, \tag{5}$$

where k represents the orientation of (110) or (111), respectively, while the stress σ_i $(i = 1, 2, 6)$ and strain u_i $(i = 1, 2, 6)$ can be derived by mechanical boundary conditions: $\partial G^k/\partial\sigma_1 = -u_1$, $\partial G^k/\partial\sigma_2 = -u_2$, and $\partial G^k/\partial\sigma_6 = -u_6$ [21, 22]. Substituting the solved σ_i, u_i, and G^k into (5), the thermodynamic potential energy of (110) and (111) oriented ferroelectric thin films can be derived, represented by $\tilde{G}^{(110)}$ and $\tilde{G}^{(111)}$ with the specific form as follows

$$\begin{aligned}\tilde{G}^{(110)} &= \alpha_1^* P_1^2 + \alpha_2^* P_2^2 + \alpha_3^* P_3^2 + \alpha_{11}^* P_1^4 + \alpha_{22}^* P_2^4 + \alpha_{33}^* P_3^4 + \alpha_{12}^* P_1^2 P_2^2 + \alpha_{13}^* P_1^2 P_3^2 + \alpha_{23}^* P_2^2 P_3^2 \\ &+\alpha_{111} P_1^6 + \alpha_{333}^* \left(P_2^6 + P_3^6\right) + \alpha_{112} P_1^4 \left(P_2^2 + P_3^2\right) + \alpha_{133}^* P_1^2 \left(P_2^4 + P_3^4\right) + \alpha_{123}^* P_1^2 P_2^2 P_3^2 \\ &+\alpha_{233}^* P_2^2 P_3^2 \left(P_2^2 + P_3^2\right) + \frac{u_m^2 \left(6S_{11} - 6S_{12} + S_{44}\right)}{4\left(S_{11} - S_{12}\right)\left(S_{11} + 2S_{12}\right) + 2S_{11}S_{44}} + G^{(8)} - P_1E_1 - P_2E_2 - P_3E_3 \end{aligned} \tag{6}$$

with

$$\begin{aligned}\alpha_1^* &= \alpha_1 - \frac{u_m\left[2\left(Q_{11}+2Q_{12}\right)\left(S_{11} - S_{12}\right) + Q_{11}S_{44}\right]}{2\left(S_{11} - S_{12}\right)\left(S_{11}+2S_{12}\right) + S_{11}S_{44}}, \\ \alpha_2^* &= \alpha_1 - \frac{u_m\left[\left(2Q_{11}+4Q_{12}+Q_{44}\right)\left(S_{11} - S_{12}\right) + Q_{12}S_{44}\right]}{2\left(S_{11} - S_{12}\right)\left(S_{11}+2S_{12}\right) + S_{11}S_{44}}, \\ \alpha_3^* &= \alpha_1 - \frac{u_m\left[\left(2Q_{11}+4Q_{12} - Q_{44}\right)\left(S_{11} - S_{12}\right) + Q_{12}S_{44}\right]}{2\left(S_{11} - S_{12}\right)\left(S_{11}+2S_{12}\right) + S_{11}S_{44}}, \\ \alpha_{11}^* &= \alpha_{11} + \frac{1}{4\left(S_{11} - S_{12}\right)\left(S_{11}+2S_{12}\right) + 2S_{11}S_{44}} \left[\left(2Q_{11}^2+4Q_{12}^2\right)S_{11} + \left(2Q_{11}^2 - 8Q_{11}Q_{12}\right)S_{12} + Q_{11}^2S_{44}\right], \\ \alpha_{22}^* &= \alpha_{112} + \frac{\alpha_{12}}{4} + \frac{1}{8\left[2\left(S_{11} - S_{12}\right)\left(S_{11}+2S_{12}\right) + S_{11}S_{44}\right]} \left[4Q_{11}^2 + Q_{44}^2S_{11} + 4Q_{11}Q_{44}S_{11}\right. \\ &\left. + Q_{11}Q_{12}\left(8S_{11} - 16S_{12}\right) + Q_{12}Q_{44}\left(4S_{11} - 8S_{12}\right) + Q_{12}^2\left(12S_{11} - 8S_{12} + 4S_{44}\right)\right], \\ \alpha_{33}^* &= \alpha_{112} + \frac{\alpha_{12}}{4} + \frac{1}{8\left[2\left(S_{11} - S_{12}\right)\left(S_{11}+2S_{12}\right) + S_{11}S_{44}\right]} \left[4Q_{11}^2S_{11} + Q_{44}^2S_{11}\right. \\ &\left. - 4Q_{11}Q_{44}S_{+}Q_{11}Q_{12}11\left(8S_{11} - 16S_{12}\right) + Q_{12}Q_{44}\left(8S_{12} - 4S_{11}\right) + Q_{12}^2\left(12S_{11} - 8S_{12} + 4S_{44}\right)\right], \\ \alpha_{12}^* &= \alpha_{12} + \frac{1}{2\left(S_{11} - S_{12}\right)\left(S_{11}+2S_{12}\right) + S_{11}S_{44}} \left[Q_{12}Q_{44}S_{11} + Q_{12}^2\left(2S_{11} - 4S_{12}\right) - 2Q_{11}^2S_{12}\right. \\ &\left. - Q_{11}Q_{44}S_{12} + Q_{11}Q_{12}\left(4S_{11} + S_{44}\right)\right] + \frac{Q_{44}^2}{2S_{44}}, \\ \alpha_{13}^* &= \alpha_{12} + \frac{1}{2\left(S_{11} - S_{12}\right)\left(S_{11}+2S_{12}\right) + S_{11}S_{44}} \left[Q_{12}^2\left(2S_{11} - 4S_{12}\right) - Q_{12}Q_{44}S_{11} - 2Q_{11}^2S_{12}\right. \\ &\left. + Q_{11}\left[Q_{44}S_{12} + Q_{12}\left(4S_{11} + S_{44}\right)\right]\right], \\ \alpha_{23}^* &= 3\alpha_{11} - \frac{\alpha_{12}}{2} + \frac{1}{4\left[2\left(S_{11} - S_{12}\right)\left(S_{11}+2S_{12}\right) + S_{11}S_{44}\right]} \left[\left(4Q_{11}^2 - Q_{44}^2\right)S_{11} + 8Q_{11}Q_{12}\left(S_{11} - 2S_{12}\right)\right. \\ &\left. + 4Q_{12}^2\left(3S_{11} - 2S_{12} + S_{44}\right)\right], \\ \alpha_{333}^* &= \frac{\alpha_{111}}{4} + \frac{\alpha_{112}}{4}, \quad \alpha_{133}^* = \frac{\alpha_{112}}{2} + \frac{\alpha_{123}}{4}, \quad \alpha_{233}^* = \frac{15\alpha_{111}}{4} - \frac{\alpha_{112}}{4}, \quad \alpha_{123}^* = 3\alpha_{112} - \frac{\alpha_{123}}{2}, \end{aligned} \tag{7}$$

where $G^{(8)}$ represents the eighth order polynomial function of P_1, P_2, and P_3, and its form is very cumbersome and omitted, and

$$\tilde{G}^{(111)} = \alpha_1^* \left(P_1^2+P_2^2\right) +\alpha_3^* P_3^2+\alpha_{11}^* \left(P_1^2+P_2^2\right)^2 +\alpha_{33}^* P_3^4+\alpha_{13}^* P_3^2 \left(P_1^2+P_2^2\right) +\alpha_{2233}^* P_2 P_3 \left(P_2^2-3P_1^2\right)$$
$$+G^{(6)}+G^{(8)}+\frac{6u_m^2}{4S_{11}+8S_{12}+S_{44}} - P_1E_1 - P_2E_2 - P_3E_3 \tag{8}$$

with

$$\alpha_1^* = \alpha_1 - \frac{u_m\left(4Q_{11}+8Q_{12}+Q_{44}\right)}{4S_{11}+8S_{12}+S_{44}}, \quad \alpha_3^* = \alpha_1 - \frac{2u_m\left(2Q_{11}+4Q_{12}-Q_{44}\right)}{4S_{11}+8S_{12}+S_{44}},$$

$$\alpha_{11}^* = \frac{1}{4}\left(2\alpha_{11}+\alpha_{12}\right)+\frac{1}{24}\Big[\frac{2\left(Q_{11}-Q_{12}+Q_{44}\right)^2}{S_{11}-S_{12}+S_{44}}+\frac{\left(4Q_{11}+8Q_{12}+Q_{44}\right)^2}{4S_{11}+8S_{12}+S_{44}}\Big],$$

$$\alpha_{33}^* = \frac{1}{6}\left[2\alpha_{11}+2\alpha_{12}+\frac{\left(Q_{44}-2Q_{11}-4Q_{12}\right)^2}{4S_{11}+8S_{12}+S_{44}}\right],$$

$$\alpha_{13}^* = 2\alpha_{11}+\frac{1}{6}\Big[\frac{\left(2Q_{11}-2Q_{12}-Q_{44}\right)^2}{S_{11}-S_{12}+S_{44}}+\frac{\left(2Q_{11}+4Q_{12}-Q_{44}\right)\left(4Q_{11}+8Q_{12}+Q_{44}\right)}{4S_{11}+8S_{12}+S_{44}}\Big],$$

$$\alpha_{2233}^* = -\frac{1}{3}\Big[2\sqrt{2}\alpha_{11}-\sqrt{2}\alpha_{12}+\frac{\left(2Q_{11}-2Q_{12}-Q_{44}\right)\left(Q_{11}-Q_{12}+Q_{44}\right)}{\sqrt{2}\left(S_{11}-S_{12}+S_{44}\right)}\Big],$$

$$G^{6)} = \frac{\alpha_{111}}{36}\Big[9P_1^6+11P_2^6-30\sqrt{2}P_2^5P_3+90P_2^4P_3^2-40\sqrt{2}P_2^3P_3^3+60P_2^2P_3^4+4P_3$$
$$+45P_1^4\Big(P_2^2+2P_3^2+2\sqrt{2}P_2P_3\Big)+15P_1^2\Big(P_2^4+4\sqrt{2}P_2^3P_3+12P_2^2P_3^2+8\sqrt{2}P_2P_3^3+4P_3^4\Big)\Big]$$
$$+\frac{\alpha_{112}}{36}\Big[9P_1^6+7P_2^6+6\sqrt{2}P_2^5P_3+16\sqrt{2}P_2^3P_3^3+24P_2^2P_3^4+9P_1^4\left(P_2^2-2\sqrt{2}P_2P_3\right)$$
$$+8P_3^6+P_1^2\Big(39P_2^4-12\sqrt{2}P_2^3P_3-48\sqrt{2}P_2P_3^3+24P_3^4\Big)\Big]$$
$$+\frac{\alpha_{123}}{108}\Big[2P_2^6+6\sqrt{2}P_2^5P_3+9P_2^4P_3-4\sqrt{2}P_2^3P_3^3-12P_2^2P_3^4+4P_3^6+9P_1^4\Big(2P_2^2+P_3^2-2\sqrt{2}P_2P_3\Big)$$
$$+6P_1^2\Big(-2P_2^4-2\sqrt{2}P_2^3P_3+3P_2^2P_3^2+2\sqrt{2}P_2P_3^3-2P_3^4\Big)\Big], \tag{9}$$

where the omitted $G^{(8)}$ is also an eighth order polynomial function.

2.2. The calculation method of electromechanical properties

Notice that the thermodynamic potential energy $\tilde{G}^k$ of oriented thin films is a function of the polarization $\boldsymbol{P}$, misfit strain u_m, electric field $\boldsymbol{E}$ and temperature T. According to the principle of minimizing potential energy, the equilibrium polarization components can be solved by setting appropriate external conditions, such as misfit strain u_m, temperature T, and electric field E_i. Thus, the phase structures of the thin films can be predicted and classified by the equilibrium polarization components. Furthermore, its electromechanical properties can be simulated, including dielectric and piezoelectric properties modulated by misfit strain. With the determining equilibrium polarization components, the dielectric constants ε_{ij} $(i,j=1,2,3)$ can be evaluated by [21, 22]

$$\varepsilon_{ij} = 1+\frac{\eta_{ij}}{\varepsilon_0}, \tag{10}$$

where $\varepsilon_0 = 8.85\times10^{-12}$ C^2/Nm^2. The relationship between η and the potential energy $\tilde{G}^k$ of the thin films is [21]

$$\eta = \begin{bmatrix} \frac{\partial^2\tilde{G}^k}{\partial P_1\partial P_1} & \frac{\partial^2\tilde{G}^k}{\partial P_1\partial P_2} & \frac{\partial^2\tilde{G}^k}{\partial P_1\partial P_3} \\ \frac{\partial^2\tilde{G}^k}{\partial P_2\partial P_1} & \frac{\partial^2\tilde{G}^k}{\partial P_2\partial P_2} & \frac{\partial^2\tilde{G}^k}{\partial P_2\partial P_3} \\ \frac{\partial^2\tilde{G}^k}{\partial P_3\partial P_1} & \frac{\partial^2\tilde{G}^k}{\partial P_3\partial P_2} & \frac{\partial^2\tilde{G}^k}{\partial P_3\partial P_3} \end{bmatrix}^{-1}. \tag{11}$$

The piezoelectric coefficients d_{in} $(i=1,2,3$ and $n=1,2,\ldots,6)$ can be written as [22]

$$d_{in} = \frac{\partial\varepsilon_n}{\partial E_i} = \frac{\partial\varepsilon_n}{\partial P_1}\eta_{i1}+\frac{\partial\varepsilon_n}{\partial P_2}\eta_{i2}+\frac{\partial\varepsilon_n}{\partial P_3}\eta_{i3}. \tag{12}$$

3. Results and discussion

3.1. Investigating the phase structure of differently oriented $K_{0.5}Na_{0.5}NbO_3$ thin films

Ferroelectric materials undergo significant changes in their physical properties due to variations in their phase structure. Consequently, this study was initiated by examining the phase structure of $K_{0.5}Na_{0.5}NbO_3$ films with varying

TABLE I

Phase structure and polarization characteristics of differently oriented $K_{0.5}Na_{0.5}NbO_3$ thin films.

Phase	Polarization components				
	(001) orientation	(110) orientation		(111) orientation	
	Global system X (or crystal system X')*	Global system X	Crystal system X'	Global system X	Crystal system X'
PE	$P_1 = P_2 = P_3 = 0$	$P_1 = P_2 = P_3 = 0$	$P_1^{'} = P_2^{'} = P_3^{'} = 0$	$P_1 = P_2 = P_3 = 0$	$P_1^{'} = P_2^{'} = P_3^{'} = 0$
Te_c	$P_1 = P_2 = 0,\ P_3 \neq 0$	$P_1 \neq 0,\ P_2 = P_3 = 0$	$P_1^{'} = P_2^{'} = 0,\ \lvert P_3^{'}\rvert \neq 0$	–	–
R_{aaa}	–	–	–	$P_1 = P_2 = 0,\ \lvert P_3\rvert \neq 0$	$P_1^{'} = P_2^{'} = P_3^{'} \neq 0$
O_{aa}	$\lvert P_1\rvert = \lvert P_2 \neq 0\rvert,\ P_3 = 0$	$P_1 = P_2 = 0,\ \lvert P_3\rvert \neq 0$	$\lvert P_1^{'}\rvert = \lvert P_2^{'}\rvert \neq 0,\ P_3^{'} = 0$	–	–
M_{aac}	$\lvert P_1\rvert = \lvert P_2\rvert \neq 0,\ \lvert P_3\rvert \neq 0$	$\lvert P_1\rvert \neq 0,\ P_2 = 0,\ \lvert P_3\rvert \neq 0$ $\lvert P_1\rvert \neq 0,\ \lvert P_2\rvert \neq 0,\ P_3 = 0$	$\lvert P_1^{'}\rvert = \lvert P_2^{'}\rvert \neq 0,\ P_3^{'} \neq 0$	$P_1 = 0,\ \lvert P_2\rvert \neq 0,\ \lvert P_3\rvert \neq 0$	$\lvert P_1^{'}\rvert = \lvert P_2^{'}\rvert \neq 0,\ P_3^{'} \neq 0$
M_{aba}	–	–	–	$\lvert P_1\rvert \neq 0,\ \lvert P_2\rvert \neq 0,\ \lvert P_3\rvert \neq 0$	$\lvert P_2^{'}\rvert \neq \lvert P_3^{'}\rvert \neq 0,\ \lvert P_1^{'}\rvert \neq 0$ $\lvert P_1^{'}\rvert \neq \lvert P_3^{'}\rvert \neq 0,\ \lvert P_2^{'}\rvert \neq 0$
T_{abc}	–	$\lvert P_1\rvert \neq \lvert P_2\rvert \neq \lvert P_3\rvert \neq 0$	$\lvert P_1^{'}\rvert \neq \lvert P_2^{'}\rvert \neq \lvert P_3^{'}\rvert \neq 0$	–	–

*Note that the (001) oriented thin films have the same polarization components in global system X and crystal system $X^{'}$.

orientations. Utilizing strain u_m ($-2\% \leq u_m \leq 2\%$) and temperature T ($0 \leq T \leq 1000$ K) as variables within the potential energy function, we determined the polarization components in an equilibrium state under the condition $E_i = 0$. Subsequently, the equilibrium polarization components were transformed into the crystal coordinate system X', facilitating the classification of phase structures based on their polarization characteristics. The resultant strain–temperature phase diagram of differently oriented $K_{0.5}Na_{0.5}NbO_3$ films is depicted in Fig. 3. Our findings revealed that the differently oriented $K_{0.5}Na_{0.5}NbO_3$ thin films exhibited seven distinct phase structures: paraelectric phase (PE), tetragonal phase (Te_c), rhombohedral phase (R_{aaa}), orthorhombic phase (O_{aa}), two monoclinic phases (M_{aac} and M_{aba}), and triclinic phase (T_{rabc}). The specific polarization components in global system X and crystal system X' associated with these phase structures are detailed in Table I. Note that the same phase structures of differently oriented films may not have the same polarization components in the global system, resulting in differences in electromechanical properties.

Based on observations from Fig. 3a, it was indicated that the (001) oriented $K_{0.5}Na_{0.5}NbO_3$ thin films primarily featured a symmetrical phase with equal in-plane polarization components, which arises from the two-dimensional clamping effect resulting from biaxial strain in the films. At elevated temperatures, the phase structure of the (001) oriented $K_{0.5}Na_{0.5}NbO_3$ film exhibited a paraelectric phase. In the vicinity of room temperature, the phase structures exhibited twice phase transitions, i.e., Te_c–M_{aac} and M_{aac}–O_{aa}, and the increased compressive strain led to the formation of a stable orthogonal O_{aa} phase, while tensile strain induced the films to assume a stable tetragonal Te_c phase. Notably, Yang et al. [23] have conducted the first-principles research on (001) oriented $K_{0.5}Na_{0.5}NbO_3$ thin films and obtained phase structures consistent with our findings. Moving on to Fig. 3b, aside from the phase structures observed in (001) oriented $K_{0.5}Na_{0.5}NbO_3$ films, an asymmetric phase with unequal polarization components in the crystal coordinate system was identified as the triclinic T_{rabc} phase. The dissimilarity in the impact of biaxial strain on the crystal axis under the crystal coordinate system, despite the similar biaxial strain under the global coordinate system, gave rise to this asymmetric phase structure. At elevated temperatures, the (110) oriented $K_{0.5}Na_{0.5}NbO_3$ thin films still exhibited the PE phase, while near room temperature, it underwent the phase transition sequence of O_{aa}–M_{aac}–T_{rabc}–M_{aac}. Comparatively, the tetragonal Te_c phase and the orthogonal O_{aa} phase of (110) oriented thin films occur in the opposite strain region, contrasting with the (001) oriented $K_{0.5}Na_{0.5}NbO_3$ thin films. Furthermore, Gui et al. [24] conducted the first-principles research on (110) oriented $BaTiO_3$ thin films, which also identified the existing O_{aa}, Tr_{abc}, and M_{aac} phases. Figure 3c highlights that the (111) oriented $K_{0.5}Na_{0.5}NbO_3$ film predominantly exhibited three symmetric phases with interchangeable polarization components in the crystal coordinate system X', driven by the identical impact of biaxial strain on all three crystal axes. Notably, the M_{aac} and M_{aba} phases coexisted in the strain region and have equivalent energies. At elevated temperatures, the (111) oriented $K_{0.5}Na_{0.5}NbO_3$ film also adopted a paraelectric phase. Additionally, it only appears once a phase transition occurs near room temperature, namely R_{aaa}–M_{aac} (or M_{aba}). Interestingly, the Curie temperature T_0 of (111) oriented $K_{0.5}Na_{0.5}NbO_3$ thin films was substantially lower than that of (001) and (110) oriented thin films. For example, when the misfit strain $u_m = -0.25\%$, the Curie temperatures T_0 of (111), (110), and (001) oriented films are 692 K, 760 K, and 950 K, respectively. Consequently, (111) oriented $K_{0.5}Na_{0.5}NbO_3$ films are better suited for applications in ferroelectric electronic components operating at lower temperatures.

Generally speaking, differences in the phase structure of $K_{0.5}Na_{0.5}NbO_3$ thin films with varying orientations exist, with symmetry decreasing in the order of (111), (001), and (110). These differences

stem from the distinct strain symmetries experienced by the crystal axes when subjected to biaxial strains, resulting in varying phase structures among $K_{0.5}Na_{0.5}NbO_3$ films with different orientations.

3.2. The electromechanical properties of differently oriented thin films

In this part, we will examine electromechanical properties, including polarization, dielectric, and piezoelectric properties of differently oriented thin $K_{0.5}Na_{0.5}NbO_3$ thin films under the misfit strain, through the above-established potential functions and calculation methods. Notice that the following polarization components, dielectric constants, and piezoelectric coefficients are in global coordinates system X, which will facilitate the analysis of in-plane and out-of-plane electromechanical coupling properties.

In scenarios where the external electric field E_i is absent, the polarization components of differently oriented $K_{0.5}Na_{0.5}NbO_3$ thin films varying with misfit strain at $T = 300$ K are displayed in Fig. 4. As indicated in Fig. 4a, the in-plane polarization components of (001) oriented $K_{0.5}Na_{0.5}NbO_3$ thin films obey the relationship $P_1 = P_2$, and there exist only Te_c, M_{aac}, and O_{aa} phases in the strain range of $-2\% < u_m < 2\%$. During the application of tensile strain, the in-plane polarization components P_1 and P_2 gradually increase while the external polarization component P_3 diminishes, while compressive strain has the contrary effect. As can be seen in Fig. 4b, the polarization vector of (110) oriented $K_{0.5}Na_{0.5}NbO_3$ thin films gradually shifts from the $\langle 110 \rangle$ direction to (110) plane during the transformation of misfit strain from compressive strain to tensile strain. Especially the strain-induced phase transformation of M_{aac}–Tr_{abc} is associated with a mutation of the polarization component P_3 at $u_m = -0.06\%$, indicating that it is of first-order. Figure 3c underscores that M_{aac} and M_{aba} coexist within the (111) oriented $K_{0.5}Na_{0.5}NbO_3$ thin films. In order to effectively simulate the electromechanical properties, we focused on the M_{aac} phase and its polarization components in subsequent research, as illustrated in Fig. 4c. At room temperature, the (111) oriented $K_{0.5}Na_{0.5}NbO_3$ films experience the R_{aaa}–M_{aac} phase transition, constituting first-order phase transition. Note that the polarization component P_2 appears and gradually increases with the increasing tensile strain, while the P_3 decreases with the increase in tensile strain, which confirms that tensile strain facilitates the in-plane polarization component and reduces the out-of-plane component P_3. Within the range of compressive strain, the (111) oriented $K_{0.5}Na_{0.5}NbO_3$ thin films achieve an improved out-of-plane polarization value, and the (111) oriented $K_{0.5}Na_{0.5}NbO_3$ thin films consistently exhibit a more stable out-of-plane polarization value compared to those with (001) and (110) orientation. These observations underscore the pivotal role of strain in regulating the polarization components of differently oriented $K_{0.5}Na_{0.5}NbO_3$ thin films. The strain-induced deformation within the crystal structure of the films results in a shift of the charge center within the crystal, thereby engendering changes in polarization. These changes in polarization, in turn, manifest as variations in electromechanical properties.

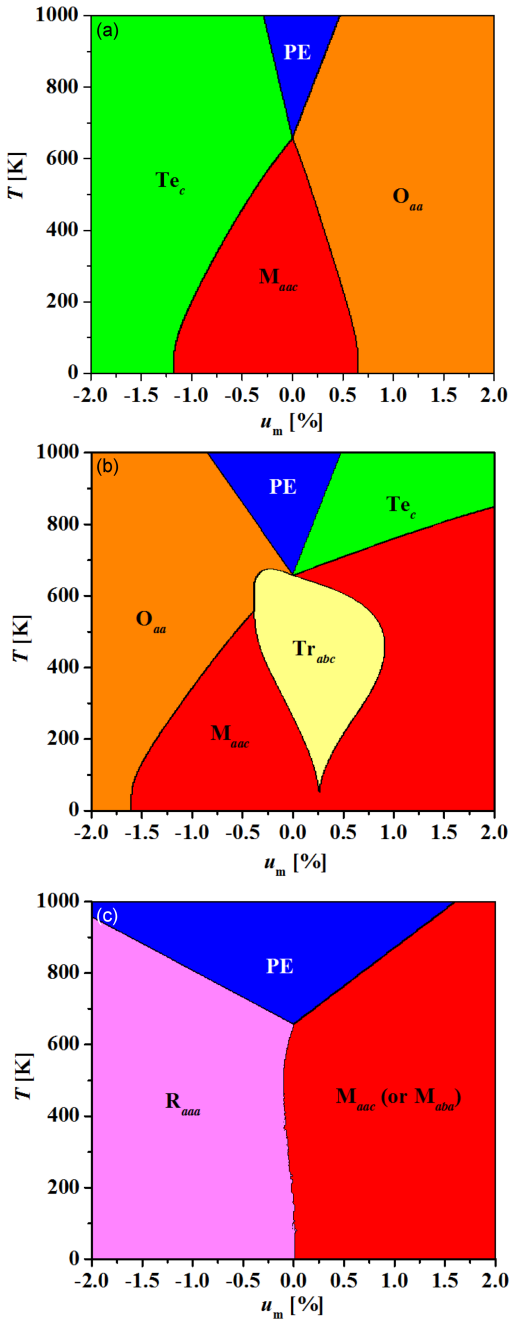

Fig. 3. Strain–temperature phase diagram of differently oriented $K_{0.5}Na_{0.5}NbO_3$ thin films: (a) phase diagram of (001) oriented films; (b) phase diagram of the (110) oriented film; (c) phase diagram of the (111) oriented film.

The properties of dielectrics significantly impact the energy storage capabilities of thin film devices, with the effectiveness of dielectric properties hinging on the magnitude of the dielectric constant. Thus, we calculate the dielectric constant ε_{33} for differently oriented $K_{0.5}Na_{0.5}NbO_3$ thin films as a function of misfit strain and temperature, as shown in Fig. 5a–c. Simultaneously, the dielectric constant curves of differently oriented $K_{0.5}Na_{0.5}NbO_3$ thin films varying with the misfit strain at $T = 300$ K are displayed in Fig. 5d–f. Figure 5a highlights that the (001) oriented $K_{0.5}Na_{0.5}NbO_3$ thin films exhibit a superior out-of-plane dielectric response at the phase boundary of M_{aac}–O_{aa} and Te_c–PE. Near room temperature, the in-plane dielectric constants ε_{11} and ε_{22}, along with the out-of-plane dielectric constant ε_{33} of the $K_{0.5}Na_{0.5}NbO_3$ thin films, attain their maximum values at the phase transformation points of Te_c–M_{aac} and M_{aac}–O_{aa}, respectively, as shown in Fig. 5d. The resulting slope of P_3 is discontinuous at the M_{aac}–O_{aa} phase boundary, while the slopes of P_1 and P_2 are discontinuous at the Te_c–M_{aac} phase boundary, as shown in Fig. 4a. In Fig. 5b, the (110) oriented $K_{0.5}Na_{0.5}NbO_3$ thin films demonstrate a superior out-of-plane dielectric response at the phase boundary of O_{aa}–PE and Tr_{abc}–M_{aac}. On the other hand, the in-plane dielectric constants ε_{11} and ε_{22}, alongside the out-of-plane dielectric constant ε_{33} of (110) oriented $K_{0.5}Na_{0.5}NbO_3$ thin films, reach their maximum values at $u_m = -1.1\%$, $u_m = -0.06\%$, and $u_m = 0.7\%$, respectively, as depicted in Fig. 5e. Similarly, these maximal dielectric responses are also obtained at discontinuous phase transition points. Figure 5c reveals that the (111) oriented $K_{0.5}Na_{0.5}NbO_3$ thin films show a commendable out-of-plane dielectric response at the R_{aaa}–PE phase boundary. Near room temperature, due to the existence of only one phase transition, the in-plane dielectric constants ε_{11} and ε_{22}, along with the out-of-plane dielectric constant ε_{33}, exhibit the enhanced dielectric responses near the phase boundary of R_{aaa}–M_{aac}, as indicated in Fig. 5f. It is indicated that dielectric peaks appear at $u_m = -0.07\%$, and there is inconspicuous dielectric response within the tensile strain range, resulting from the lack of phase transitions. Comparing the dielectric constant ε_{33} of the three differently oriented $K_{0.5}Na_{0.5}NbO_3$ thin films, it is noted that the dielectric values range from 100 to 500 in most regions, which closely align with experimental measurements [25]. Further comparison shows that the (001) and (110) oriented $K_{0.5}Na_{0.5}NbO_3$ thin films exhibit excellent dielectric properties near the phase transition point at room temperature, featuring a dielectric constant exceeding 2500, surpassing the dielectric constant of (111) oriented $K_{0.5}Na_{0.5}NbO_3$ thin films. These are also caused by the large variation in the polarization slopes of the (001) and (110) oriented thin films near the phase transition boundary. In Fig. 5e–f, it is demonstrated that (001) and (110) oriented $K_{0.5}Na_{0.5}NbO_3$ thin films generally exhibit enhanced in-plane dielectric properties within the compressive strain and improved out-of-plane dielectric properties within the tensile strain. These findings underscore the effectiveness of strain regulation in modulating the dielectric properties of differently oriented $K_{0.5}Na_{0.5}NbO_3$ thin films.

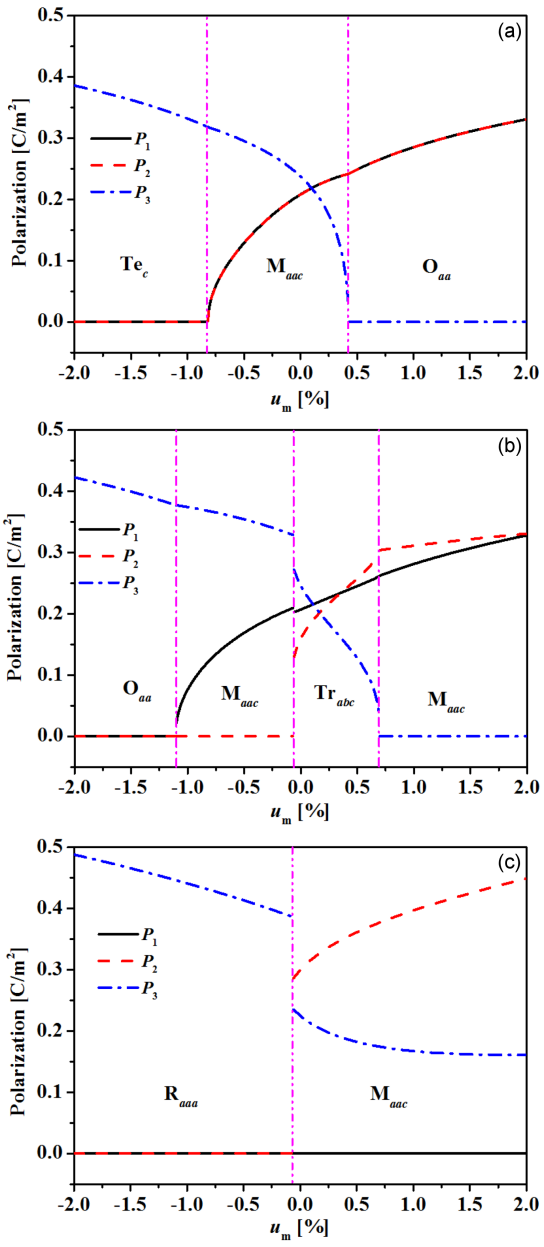

Fig. 4. The polarization components of differently oriented $K_{0.5}Na_{0.5}NbO_3$ thin films varying with misfit strain at $T = 300$ K; (a) polarization components of (001) oriented films; (b) polarization component of the (110) oriented films; (c) polarization component of the (111) oriented films.

In the following analysis, we explore piezoelectric properties of differently oriented $K_{0.5}Na_{0.5}NbO_3$ thin films, thus, the gradient diagrams of the piezoelectric coefficient d_{33} concerning strain and

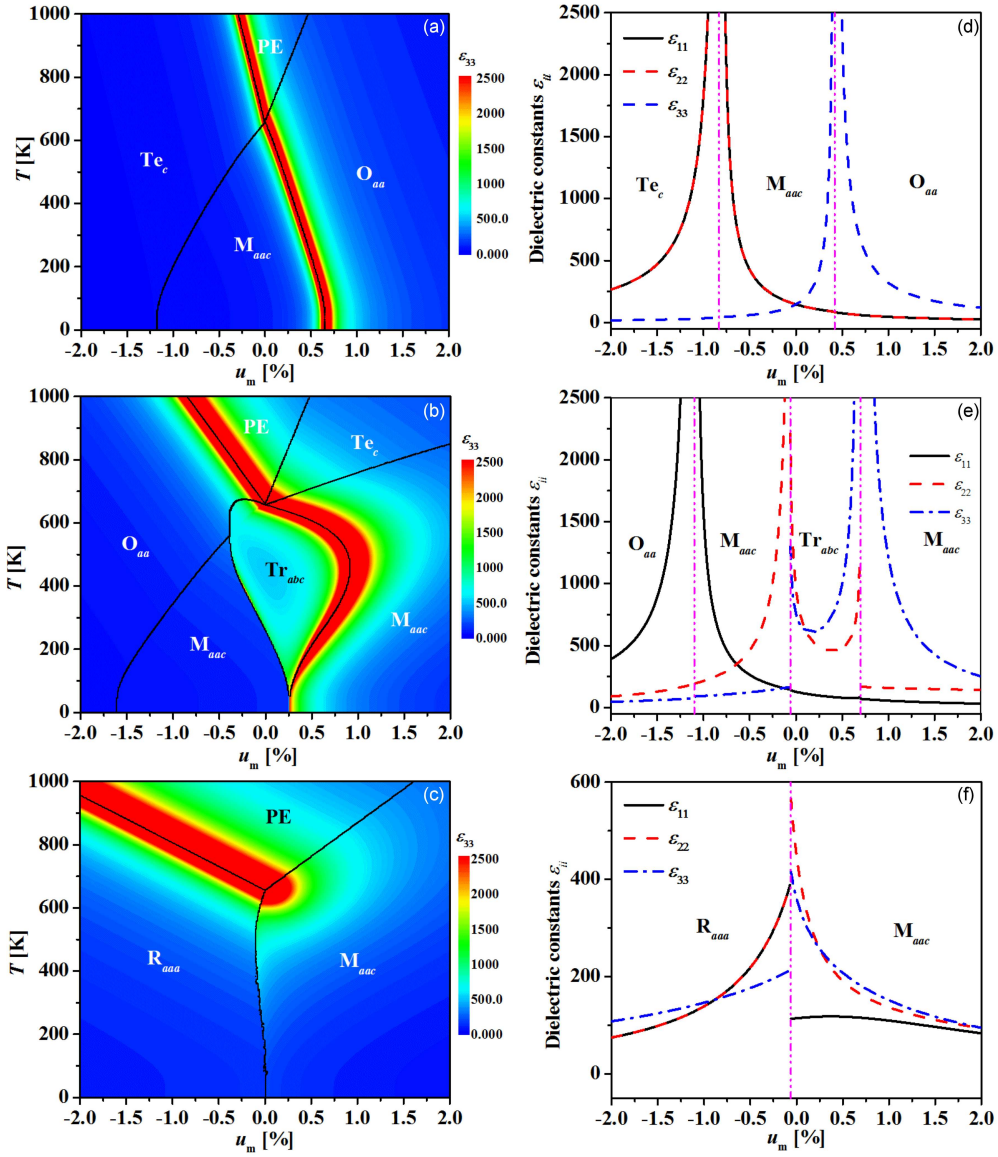

Fig. 5. (a–c) The dielectric constant ε_{33} of differently oriented $K_{0.5}Na_{0.5}NbO_3$ thin films as a function of misfit strain and temperature. (d–f) The dielectric constant curves of differently oriented $K_{0.5}Na_{0.5}NbO_3$ thin films varying with the misfit strain: (a) and (d) for (001) orientation; (b) and (e) for (110) orientation; (c) and (f) for (111) orientation.

temperature variations are presented in Fig. 6a–c. Additionally, the piezoelectric coefficients d_{15} and d_{33} of differently oriented $K_{0.5}Na_{0.5}NbO_3$ thin films varying with the misfit stain at $T = 300$ K are shown in Fig. 6d–f. Figure 6a reveals that the (001) oriented $K_{0.5}Na_{0.5}NbO_3$ films exhibit superior out-of-plane piezoelectric response at the boundary of M_{aac}–O_{aa} and Te_c–PE. Near room temperature, the (001) oriented $K_{0.5}Na_{0.5}NbO_3$ thin film displays a substantial in-plane piezoelectric response near the Te_c–M_{aac} phase boundary and a more pronounced out-of-plane dielectric response near the M_{aac}–O_{aa} phase boundary, as indicated in Fig. 6d. In Fig. 6b, the (110) oriented $K_{0.5}Na_{0.5}NbO_3$ film demonstrates an enhanced out-of-plane piezoelectric response near O_{aa}–PE, M_{aac}–Tr_{abc}, and Tr_{abc}–M_{aac} phase boundaries. At $T = 300$ K, the piezoelectric coefficient d_{15} of (110) oriented $K_{0.5}Na_{0.5}NbO_3$ thin films exhibits a substantial piezoelectric response near the O_{aa}–M_{aac} phase boundary and an improved piezoelectric coefficient d_{33} near the Tr_{abc}–M_{aac} phase transition point, as shown in Fig. 6e. In Fig. 6c, it is indicated that the (111) oriented $K_{0.5}Na_{0.5}NbO_3$ thin films achieve a robust external piezoelectric response at the transition boundary R_{aaa}–PE. Near room temperature, the (111) oriented $K_{0.5}Na_{0.5}NbO_3$ thin films experience only one phase transition R_{aaa}–M_{aac}, and their piezoelectric coefficients d_{15} and d_{33} exhibit substantial piezoelectric responses, as depicted in Fig. 6f. Upon comparing the piezoelectric properties of three oriented

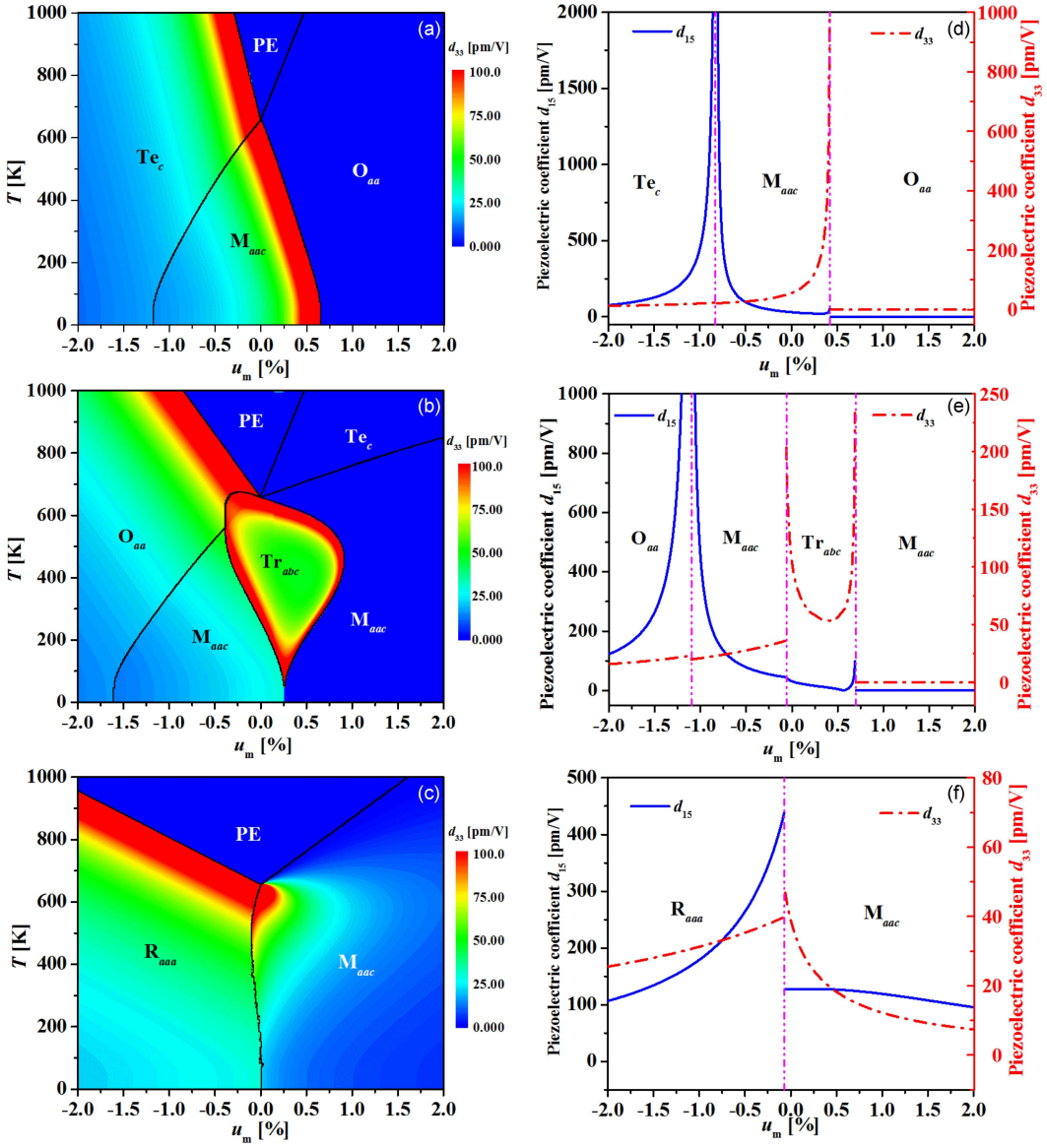

Fig. 6. (a–c) The piezoelectric coefficient d_{33} of differently oriented $K_{0.5}Na_{0.5}NbO_3$ thin films as a function of strain and temperature. (d–f) The piezoelectric coefficients of differently oriented $K_{0.5}Na_{0.5}NbO_3$ thin films varying with the misfit strain: (a) and (d) for (001) orientation; (b) and (e) for (110) orientation; (c) and (f) for (111) orientation.

thin films, we observed that the piezoelectric coefficients d_{33} in most regions varying with misfit strain and temperature fall within the range of 25–75 pm/V, which closely align with experimental measurements [26–28]. Notably, near room temperature, the out-of-plane piezoelectric properties of (001) oriented $K_{0.5}Na_{0.5}NbO_3$ thin films significantly outperform that of (110) and (111) oriented $K_{0.5}Na_{0.5}NbO_3$ thin films, with the piezoelectric coefficient d_{33} exceeding 1000 pm/V. Both (110) and (001) oriented $K_{0.5}Na_{0.5}NbO_3$ thin films exhibit superior in-plane piezoelectric properties compared to (111) oriented $K_{0.5}Na_{0.5}NbO_3$ thin films, with the piezoelectric coefficient d_{15} surpassing 2000 pm/V. Similarly, the (001) and (110) oriented $K_{0.5}Na_{0.5}NbO_3$ thin films generally exhibit superior in-plane piezoelectric properties within the compressive strain region and enhanced out-of-plane piezoelectric properties within the tensile strain area. Thus, this underscores the significant influence of strain and temperature regulation on piezoelectric properties, paving the way for the fabrication of devices with high piezoelectric properties by manipulating these parameters.

4. Conclusions

In summary, the eighth-order thermodynamic potential energy function and the method of electromechanical properties for differently oriented $K_{0.5}Na_{0.5}NbO_3$ thin films have been deduced by

using the thermodynamic theory, and then the phase structures and electromechanical properties of differently oriented $K_{0.5}Na_{0.5}NbO_3$ thin films have been investigated. Our findings reveal notable distinctions in the phase structure of $K_{0.5}Na_{0.5}NbO_3$ thin films, with decreasing symmetry observed in the order of (111), (001), and (110) orientations, and these microphase structural variances translate into distinct electromechanical properties among the orientations. Moreover, it is observed that differently oriented $K_{0.5}Na_{0.5}NbO_3$ thin films exhibit commendable dielectric and piezoelectric properties within specific phases. Specifically, (001) and (110) oriented $K_{0.5}Na_{0.5}NbO_3$ thin films consistently demonstrate superior in-plane dielectric and piezoelectric properties within the reasonable compressive strain and enhanced out-of-plane dielectric and piezoelectric properties within the reasonable tensile strain. Near room temperature, the (001) and (110) oriented $K_{0.5}Na_{0.5}NbO_3$ thin films outperform (111) oriented $K_{0.5}Na_{0.5}NbO_3$ thin films in terms of dielectric properties, featuring a dielectric constant exceeding 2500. Furthermore, (001) and (110) oriented $K_{0.5}Na_{0.5}NbO_3$ thin films excel in in-plane piezoelectric properties, with their piezoelectric coefficient d_{15} reaching a peak value exceeding 2000 pm/V. Notably, (001) oriented $K_{0.5}Na_{0.5}NbO_3$ thin films exhibit superior out-of-plane piezoelectric properties compared to other orientations, with a remarkable piezoelectric coefficient d_{33} exceeding 1000 pm/V. These results underscore the significant impact of strain and temperature regulation on electromechanical properties. Meanwhile, by strategically adjusting these parameters, it becomes feasible to fabricate devices with high piezoelectric properties.

Acknowledgments

This work was supported by the Youth Science Foundation of Xinjiang Second Medical College, China (grants QK202202 and QK202201).

References

[1] E. Cross, *Nature* **432**, 24 (2004).

[2] Y.-J. Dai, X.-W. Zhang, K.-P. Chen, *Appl. Phys. Lett.* **94**, 042905 (2009).

[3] B. Wang, H.N. Chen, J.J. Wang, L.Q. Chen, *Appl. Phys. Lett.* **115**, 092902 (2019).

[4] C. Kang, J.-H. Park, D. Shen, H. Ahn, M. Park, D.-J. Kim, *J. Sol-Gel Sci. Technol.* **58**, 85 (2011).

[5] S. Sharma, A. Kumar, V. Gupta, M. Tomar, *Vacuum* **160**, 233 (2019).

[6] S. Pradhan, M. Rath, A. David, D. Kumar, W. Prellier, M.R. Rao, *ACS Appl. Mater. Interfaces* **13**, 36407 (2021).

[7] D. Liu, G. Bai, C. Gao, *J. Appl. Phys.* **127**, 154101 (2020).

[8] G. Bai, H. Yu-Hang, G. Cun-Fa, *Acta Phys. Sin.* **71**, 8 (2022).

[9] N.B. He, Q. Li, C. Lei, J. Pan, D. L. Shan, K. Pan, Y. Y. Liu, *Int. J. Solids Struct.* **252**, 111808 (2022).

[10] H. Wu, X. Ma, Z. Zhang, J. Zeng, J. Wang, G. Chai, *AIP Adv.* **6**, 015309 (2016).

[11] J. Qiu, Z. Chen, X. Wang, N. Yuan, J. Ding, *Solid State Commun.* **236**, 1 (2016).

[12] A. Tagantsev, N. Pertsev, P. Muralt, N. Setter, *Phys. Rev. B* **65**, 012104 (2001).

[13] M.J. Haun, E. Furman, S.J. Jang et al., *Ferroelectrics* **99**, 13 (1989).

[14] J.L. Peng, D.L. Shan, Y.Y. Liu, K. Pan, C. Lei, N.B. He, Z. Zhang, Q. Yang, *npj Comput. Mater.* **4**, 66 (2018).

[15] H. Pohlmann, J.-J. Wang, B. Wang, L.-Q. Chen, *Appl. Phys. Lett.* **110**, (2017).

[16] M.-J. Zhou, B. Wang, K. Peng, H.-X. Liu, L.-Q. Chen, C.-W. Nan, *Acta Mater.* **248**, 118777 (2023).

[17] J.H. Qiu, Z.H. Chen, X.Q. Wang et al., *Chinese Phys. B* **25**, 057701 (2016).

[18] N. Pertsev, A. Zembilgotov, A. Tagantsev, *Ferroelectrics* **223**, 79 (1999).

[19] Y.Y. Liu, R.K. Vasudevan, K. Pan et al., *Nanoscale* **4**, 3175 (2012).

[20] Y.Y. Liu, L. Yang, J.Y. Li, *J. Appl. Phys.* **113**, 183524 (2013).

[21] D.L. Shan, C. Lei, Y. Cai, K. Pan, Y.Y. Liu, *Int. J. Solids Struct.* **216**, 59 (2021).

[22] Y.Y. Liu, Z. Zhu, J.-F. Li, J.Y. Li, *Mech. Mater.* **42**, 816 (2010).

[23] D. Yang, Q. Chai, L. Wei, X. Chao, Z. Yang, *Phys. Chem. Chem. Phys.* **19**, 27368 (2017).

[24] Z. Gui, S. Prosandeev, L. Bellaiche, *Phys. Rev. B* **84**, 214112 (2011).

[25] L. Cakare-Samardzija, B. Malic, M. Kosec, *Ferroelectrics* **370**, 113 (2008).

[26] R. Castañeda-Guzmán, R. López-Juárez, J. Gervacio, M. Cruz, S.D. de la Torre, S. Pérez-Ruiz, *Thin Solid Films* **636**, 458 (2017).

[27] A. Mahajan, R. Pinho, M. Dolhen, M.E. Costa, P.M. Vilarinho, *Langmuir* **32**, 5241 (2016).

[28] Q. Yu, J.F. Li, W. Sun et al., *J. Appl. Phys.* **113**, 024101 (2013).